

Exploring Pose-Guided Imitation Learning for Robotic Precise Insertion

Han Sun, Yizhao Wang, Zhenning Zhou, Shuai Wang, Haibo Yang, Jingyuan Sun and Qixin Cao

Abstract—Recent studies have proved that imitation learning shows strong potential in the field of robotic manipulation. However, existing methods still struggle with precision manipulation task and rely on inefficient image/point cloud observations. In this paper, we explore to introduce SE(3) object pose into imitation learning and propose the pose-guided efficient imitation learning methods for robotic precise insertion task. First, we propose a precise insertion diffusion policy which utilizes the relative SE(3) pose as the observation-action pair. The policy models the source object SE(3) pose trajectory relative to the target object. Second, we explore to introduce the RGBD data to the pose-guided diffusion policy. Specifically, we design a goal-conditioned RGBD encoder to capture the discrepancy between the current state and the goal state. In addition, a pose-guided residual gated fusion method is proposed, which takes pose features as the backbone, and the RGBD features selectively compensate for pose feature deficiencies through an adaptive gating mechanism. Our methods are evaluated on 6 robotic precise insertion tasks, demonstrating competitive performance with only 7 – 10 demonstrations. Experiments demonstrate that the proposed methods can successfully complete precision insertion tasks with a clearance of about 0.01 mm. Experimental results highlight its superior efficiency and generalization capability compared to existing baselines. Code will be available at <https://github.com/sunhan1997/PoseInsert>.

I. INTRODUCTION

Robotic precise insertion in unstructured environments is a complex manipulation problem from the aspects of sensing and control [1].

To train closed-loop insertion policies, the previous works [2], [3], [4], [5] proposed part insertion approaches that combine reinforcement learning (RL) with force information or tactile information, which struggle with sparse rewards and face significant challenges in bridging the sim-to-real gap. Moreover, it is often difficult for these methods to generalize to varying object poses. Policy learning with RL can be unstable [6], and random exploration makes data collection inefficient, shown in Fig. 1. These issues limits their practical applicability in real-world. In contrast, imitation learning-based robotic manipulation methods is more tractable and only require data collection for training.

Imitation learning has demonstrated strong capabilities in acquiring complex manipulation skills and significantly reducing engineering complexity. Imitation learning methods

Han Sun, Yizhao Wang, Zhenning Zhou and Qixin Cao are with the School of Mechanical Engineering, Shanghai Jiao Tong University, Shanghai 200240 China (e-mail: sunhan1997@sjtu.edu.cn; wangyizhao@sjtu.edu.cn; zhenning.zhou@sjtu.edu.cn; qxcao@sjtu.edu.cn). Shuai Wang and Haibo Yang are with the Shanghai Huawei Technologies Co., Ltd., Shanghai 201799 China (e-mail: wangshuai212@huawei.com; yanghaibo27@huawei.com).

Jingyuan Sun is with the Shanghai Huawei Technologies Co., Ltd., Shanghai 201799 China (corresponding author to provide phone: 18603680666; fax: none; e-mail: sunj549@gmail.com).

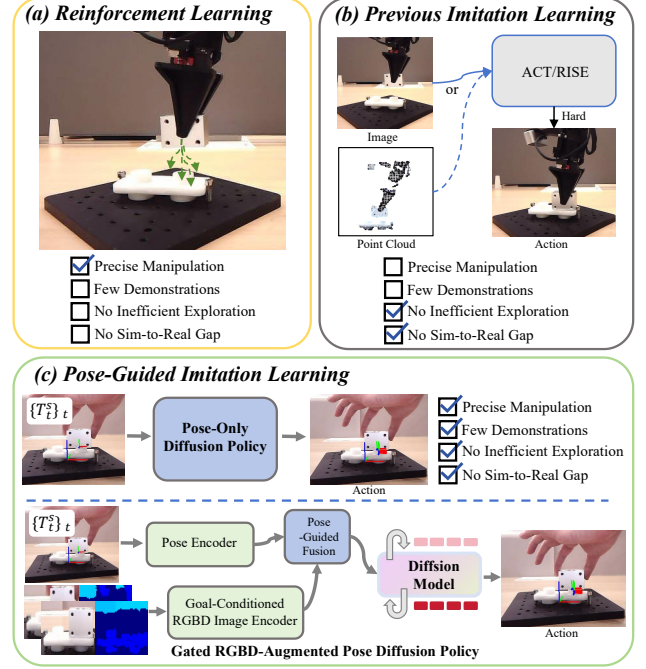


Fig. 1. As depicted in (a), RL Methods face challenges of inefficient exploration and sim2real gap. Recent studies in (b) utilize the image/point cloud as input to learn action, which can't address the precise manipulation with few demonstrations. In contrast, our framework in (c), achieves precise manipulation with few demonstrations.

leverage supervised learning to train robust policies, and integrates perception, planning, and execution into a continuous learning process.

Previous work [7], [8], [9], [10] has utilized raw RGB or point cloud inputs for end-to-end visuomotor policy training, shown in Fig. 1. However, these representations make it difficult to generalize to various viewing angles and out-of-distribution spatial configurations. In addition, these methods requires dozens or hundreds of demonstrations per task [7], [11], [12] to collect a sufficiently diverse training dataset, leading to inefficient data utilization and a significant data collection burden, especially for precise manipulation. To address these problems, object-centric methods that extracting object-centric information from visual observation, such as object detection [13], 6D object poses [14], [15], 2D or 3D flows [16], [17], [18], to serve as inputs for downstream policies. Unfortunately, most studies assume that the object is in several fixed poses. When the object pose changes, most algorithms are unable to adapt.

On the other hand, most works can not solve the precise manipulation task. Although [14] proposed category-level behavior cloning for insertion task, it must identify keypose

as the start of the behavior cloning process and use expensive industrial camera. [19] learned precise contact-rich manipulation by a single demonstration, which was unable to generalize to unseen pose configurations. Therefore, developing an imitation learning method to address precise insertion tasks, which maintains robustness to pose disturbances and learns new tasks from few demonstrations, remains a significant challenge.

To address these issues, we explore to design the imitation learning method for precise insertion task, which learns new tasks from few demonstrations. In this letter, we utilize the SE(3) object pose representation as the observation-action pair instead of raw RGB or point cloud observations. We explore the pose-guided imitation learning from two perspectives: (1) The policy only employs the source object SE(3) pose relative to the target object as observation, and predicts the future relative SE(3) pose trajectory as action. (2) Considering the noise of pose estimation, based on the above policy, RGBD information is introduced as observation to assist pose features for action prediction. To explore the performance of the proposed methods, we design 6 insertion tasks with varying precision. Note that our study focuses on complex trajectory modeling during the insertion process and doesn't use force information. We use an ALOHA-like robotic arm that exhibits passive compliance during task execution.

In summary, the contributions of our work are as follows.

- We propose a pose-guided imitation learning method to address robotic precise insertion tasks, introducing a disentangled pose encoder to enhance feature representation for complex action prediction.
- To mitigate the impact of pose estimation noise, we incorporate RGBD information into the pose-guided imitation learning. Specifically, we propose a goal-conditioned RGBD image encoder to capture the discrepancy between the current state and goal state. Furthermore, we propose a pose-guided residual gated fusion module, where pose features serve as the backbone, while RGBD features selectively compensate for pose feature deficiencies through an adaptive gating mechanism.
- Our experiments demonstrate that the proposed imitation learning methods achieve strong generalization and robustness in robotic precision insertion tasks, requiring only 7–10 demonstrations for effective learning.

II. RELATED WORK

A. Robotic Precise Insertion

Robotic precise insertion tasks remain one of the most challenging and extensively researched problems in the field of robotics [1], [20], [21], and have been widely studied [2], [22], [23]. [2] explored part insertion tasks using tactile sensors and reinforcement learning. [3], [4], [5] proposed part insertion approaches that combine reinforcement learning with force information. These methods struggle with generalizing to varying object poses and face challenges transitioning from sim-to-real. Furthermore, random exploration

makes data collection inefficient. These issues limits their practical applicability in real-world. Therefore, it is necessary to develop an efficient and strong generalization method for real-world robotic precise insertion.

B. End-to-end Imitation Learning

Imitation learning has achieved significant advancements [8], [9], [24], [25], especially in the complex robotic manipulation tasks. These methods directly map raw sensory observations to corresponding robot action predictions by learning from expert demonstrations. Specifically, ACT [24] uses transformer backbones and ResNet image encoders to model the variability of human data. Diffusion Policy [8] directly utilizes diffusion process to express multi-modal action distributions generatively. Some researchers [9], [25], [26] explore the incorporation of 3D information to imitation learning. DP3 [26] leverages 3D perception in robotic manipulation policies. RISE [9] predicts continuous actions directly from point cloud with a sparse 3D encoder. Although previous studies have introduced 3D information into imitation learning frameworks, they still fail to incorporate object pose information explicitly and address the precise insertion tasks. Instead, these 3D data-based methods introduces redundant information and increases computational complexity, ultimately leading to inefficient learning and limited generalization capabilities.

C. Object-Centric Imitation Learning

Object-centric methods that extracting object-centric information from visual observation, such as object detection [13], point tracking [27], 6D object poses [14], [15], 2D or 3D flows [16], [17], [18], to serve as inputs for downstream policies. Among these, using 6D object pose as observations offers distinct advantages. The object pose provides a compact geometric representation of the object, with its low-dimensional nature significantly reducing the complexity of policy learning. In addition, pose information is inherently robust to perceptual variations (e.g., background clutter, lighting changes, or partial occlusion) [15].

In this paper, we explore to design the pose-guided efficient imitation learning method, which utilizes the relative SE(3) poses as observation-action pair for robotic precise insertion tasks.

III. PROPOSED APPROACH

In this section, we present a detailed description of the proposed pose-only diffusion policy and gated RGBD-augmented pose diffusion policy. Additionally, we introduce the corresponding human demonstration data collection methods tailored for each approach.

A. Pose-Only Diffusion Policy

In this paper, we opt for 6D object pose as the object-centric representation, which depicts the full 6D state information of rigid objects throughout the episode. The insertion task involves a set of objects $v = \{v^s, v^t\}$, consisting of a graspable source object v^s and a target object v^t . In practice,

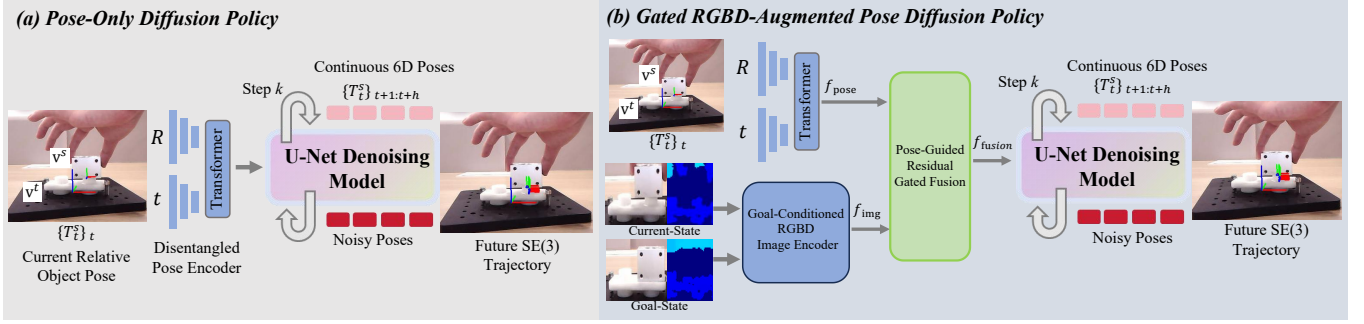


Fig. 3. **Pipeline of the pose-guided imitation learning methods.** (a) For the **pose-only diffusion policy**, current source object pose relative to the target object $\{T_t^s\}_t$ is considered as observation. The disentangled pose encoder is applied to extract the pose features. Then, diffusion policy predicts the future relative $SE(3)$ trajectory $\{T_t^s\}_{t+1:t+h}$. (b) For the **gated RGBD-augmented pose diffusion policy**, current relative object pose $\{T_t^s\}_t$ is fed to the disentangled pose encoder to get the f_{pose} , the current RGBD image patch is sent to goal-conditioned RGBD image encoder to obtain the f_{img} . And the residual gated fusion module uses image features to assist pose features. The enhanced fusion feature f_{fusion} is fed to diffusion policy to predict the future relative $SE(3)$ trajectory $\{T_t^s\}_{t+1:t+h}$.

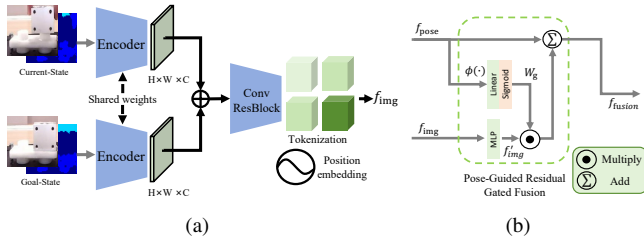


Fig. 4. (a) Goal-conditioned RGBD image encoder. We employ the [28]’s refinenet to extract the RGBD features. The two branch inputs of the refinenet are changed to the current RGBD image patch and the goal RGBD image patch, respectively. (b) Pose-guided residual gated fusion module. The MLP layer consists of a linear transformation, LayerNorm, and ReLU activation.

affected by hand-eye calibration error or robotic repeatability error, which is analyzed in Section. IV-E.

B. Gated RGBD-Augmented Pose Diffusion Policy

In Section III-A, the proposed pose-only diffusion policy learns the $SE(3)$ pose trajectory of the source object relative to the target object, effectively modeling complex insertion trajectories. This method relies on the accuracy of 6D pose estimation. As shown in Fig. 2 (a), when the pose estimation algorithm provides precise 6D poses for both the source and target objects, the method achieves strong performance and demonstrates impressive generalization across diverse scenarios, which is shown in Section IV-B. However, as shown in Fig. 2 (b), under noisy pose conditions, the model may struggles to learn meaningful trajectories from demonstrations, which is shown in Table I and Section IV-B. To address this limitation, we propose augmenting the framework with RGB-D information to dynamically correct pose errors and enhance trajectory robustness.

Human Demonstration Data Collection Similar to Section III-A, in addition to the relative pose trajectory $\hat{\tau} = \{T_t^s\}_i$, we capture RGB-D images during insertion. The 6D poses of source/target objects are estimated, along with their axis-aligned bounding boxes:

$$B_s = ((x_s^1, y_s^1), (x_s^2, y_s^2)), B_t = ((x_t^1, y_t^1), (x_t^2, y_t^2)) \quad (3)$$

The union bounding box is computed as:

$$B = ((\min(X), \min(Y)), (\max(X), \max(Y))) \quad (4)$$

where $X = \{x_s^1, x_s^2, x_t^1, x_t^2\}$ and $Y = \{y_s^1, y_s^2, y_t^1, y_t^2\}$. This ensures the cropped RGB-D patches $\{I\}_i$ encapsulate both objects, enhancing model generalization.

Goal-Conditioned RGBD Image Encoder Inspired by [28] and [33], we propose a goal-conditioned RGBD image encoder to capture the discrepancy between current and goal states, further enhancing the pose diffusion policy while achieving data-efficient training. Both the current I_c and goal I_g observations are cropped and resized into 320×320 before sending to the network. As shown in Fig. 4 (a), the goal observation I_g is explicitly fed into the network through channel-wise concatenation with the current observation I_c , enabling direct learning of the current-to-goal discrepancy. Following the RefineNet architecture in FoundationPose [28], we employ a shared CNN encoder to extract and align low-level features (e.g., edges, geometric structures) from both I_c and I_g . The concatenated features are then processed by residual blocks [34] and tokenized into patches with position embeddings [35]. This architecture facilitates the extraction of distinctive feature representations that capture the discrepancy between current and goal states, while simultaneously reducing computational overhead.

Pose-Guided Residual Gated Fusion The introduction of RGBD observation aims to mitigate the influence of pose estimation noise, thereby refining the motion prediction of the source object. To achieve this, we propose a pose-guided residual gated fusion module. In this module, the pose features serve as the primary features, while the gating weights for image features are dynamically computed based on the pose features. Through the gating mechanism, image features adaptively compensate for the limitations of pose features, ensuring a robust fusion of multimodal information. This design philosophy ensures that visual cues dynamically intervene according to pose features.

The pose features from the disentangled pose encoder are defined as $f_{pose} \in \mathbb{R}^{B \times 128}$. As shown in Fig. 4 (b), the image

features from the goal-conditioned RGBD image encoder are defined as $f_{img} \in \mathbb{R}^{B \times 1200}$. The image features are sent to a MLP layer, which compresses f_{img} to the same dimensions $f'_{img} \in \mathbb{R}^{B \times 128}$ as the pose features. The gate layer $\phi(\cdot)$ consists of a linear transformation followed by a Sigmoid activation function. The pose features are processed through the gate layer to generate gating weights W_g ,

$$W_g = \phi(f_{pose}) \quad (5)$$

which enables the model to dynamically modulate visual feature contributions based on the current pose state through adaptive feature selection. The gating weights W_g are element-wise multiplied with the image features f'_{img} , followed by residual connection fusion with the pose features f_{pose} .

$$f_{fusion} = f_{pose} + W_g \odot f'_{img} \quad (6)$$

where \odot represents elementwise multiplication. This architecture preserves the dominance of geometric priors while enabling conditional feature integration. The gating mechanism facilitates finer-grained cross-modal information flow control compared to conventional concatenation or additive operations. Crucially, using pose features as control signals aligns with the geometry-driven characteristics inherent in insertion tasks.

Diffusion Policy Similar to Section III-A, we use the diffusion process to generate the $SE(3)$ pose trajectory of the source object relative to the target object. The observation input \mathbf{O}_t is defined as the current $SE(3)$ relative pose $\{T_t^s\}_t \in SE(3)$ and RGBD image patch $\{I_t\}_t \in \mathbb{R}^{H \times W \times 4}$. The action output \mathbf{A}_t is the future relative pose over a prediction horizon of h time steps: $\{T_t^s\}_{t+1:t+h} \in SE(3)^h$. The loss function for diffusion policy and end-effector action generation follows the same formulation as in Section. III-A.

IV. RESULT AND EXPERIMENTS

In this section, we provide our implementation details and experimental setup, evaluate the proposed methods and present results compared with the state-of-the-art imitation learning methods in various real-world experiments. Then, we conduct ablation studies to evaluate the proposed modules, including the Disentangled Pose Encoder (DPE), Goal-Conditioned RGBD Image Encoder (GIE) and Pose-Guided Residual Gated Fusion (PRGF). Furthermore, we also provide the further analysis.

A. Experimental Setup

Implementation Details. All the experiments are performed on the Cobot Mobile ALOHA, a robot using the Mobile ALOHA system design [24] and manufactured by agilex.ai (Fig. 5 (a)). It is important to note that although this robot is not equipped with force sensors, it exhibits passive compliance during task execution, which means that this robot can perform contact-rich tasks in a safe situation. An Orbbeo Dabai camera, the front camera in Fig. 5 (a), is used as a vision sensor to observe the objects on the table. We collect 7 – 10 demonstrations for each task. During the data

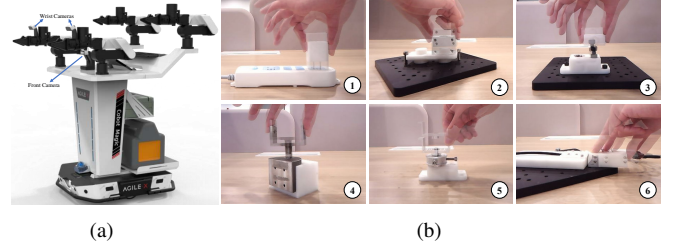


Fig. 5. (a) Cobot Mobile ALOHA for experiments. (b) There are 6 precise insertion tasks for the real-world experiments.

TABLE I
THE SUCCESS RATE (%) OF OUR METHODS AND BASELINES.

Methods	1	2	3	4	5	6	Average
ACT [24]	10	0	0	0	0	0	1.7
RISE [9]	20	0	0	0	0	0	3.3
SPOT [15]	100	70	90	90	70	10	71.7
PoseDP	100	100	90	100	70	30	81.7
RPDP	100	100	90	90	70	100	91.7

collection process, the target object pose remains unchanged to reduce the influence of pose estimation noise. And all data are collected with 30Hz. All the experiments are conducted on a single NVIDIA RTX4060 GPU. We train the networks using AdamW optimizer with a batch size of 80 and an initial learning rate of $3e - 4$. The training epoch is 2000.

Task Description. As illustrated in Fig. 5 (b), we carefully design 6 precise insertion tasks, including plug into socket (task 1), metal part into base (task 2,3,4,5) and USB (Type-C) insertion. The measured clearances are 0.28 mm for task 2, 0.08 mm for task 3, 0.03 mm for task 4, and 0.01 mm for task 5. The difficulty of tasks 1 to 6 gradually increases.

Evaluation Metrics. We employ the success rate (SR) as the evaluation metric, which is calculated by dividing successful trials by total trials. Each policy is tested for 10 consecutive trials to evaluate its performance.

Baselines. We compare with the state-of-the-art imitation learning methods: ACT [24], RISE [9] and SPOT [15]. For ACT and RISE, we collect 50 demonstrations for each task. Since SPOT is not open-source, we implemented reproduction codes using MLP and Diffusion Policy approaches, collecting 10 demonstrations per task for training.

B. Pose-Only Diffusion Policy

Table I presents the quantitative evaluation comparing the pose-only diffusion policy (PoseDP), Gated RGBD-Augmented Pose Diffusion Policy (RPDP) with baselines when objects are positioned within the train distribution range, while Table II demonstrates the comparative results for out-of-distribution conditions.

As shown in Table I, the ACT and RISE failed in any of the 10 trials across the tasks 2 to 6. Due to the larger insertion clearance in task 1, ACT achieves one successful insertion, while RISE succeeded twice. Table II further reveals that both methods failed completely across all tasks under out-of-distribution conditions, highlighting their limitations in generalization of precision manipulation. SPOT employs relative pose as observation input, achieving a comparable success rate of 71.7% under standard conditions, and maintaining

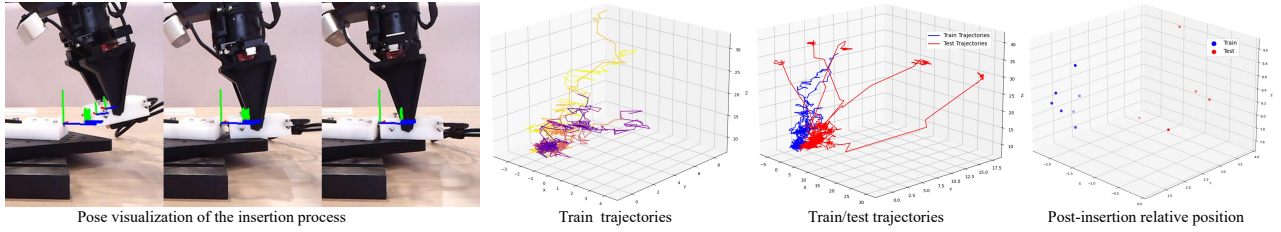


Fig. 6. Visualization of train/test trajectories for task 6 (Unit: Millimeter).

TABLE II
THE SUCCESS RATE (%) OF OUR METHODS AND BASELINES.
(OUT OF DISTRIBUTION)

Methods	1	2	3	4	5	6	Average
ACT [24]	0	0	0	0	0	0	0
RISE [9]	0	0	0	0	0	0	0
SPOT [15]	90	70	80	70	50	10	61.7
PoseDP	90	100	90	90	60	30	76.7
RPDP	80	90	70	90	60	80	78.3

61.7% average success rate when handling out-of-distribution cases. SPOT achieves the same performance as the PoseDP w/ MLP, shown in Table III and Table IV. In contrast, the PoseDP with disentangled pose encoder demonstrates superior performance, achieving an 81.7% average success rate under standard conditions and maintaining 76.7% average success rate with out-of-distribution cases, outperforming SPOT in both scenarios.

We observed that ACT learned the downward insertion trend but failed to refine the hole-searching trajectory, even with wrist-camera feedback in task 2. This suggests its visual encoder struggles to extract features relevant to the fine-grained trajectory. The absence of point cloud data prevents RISE from accurately localizing the contact region. Consequently, the model fails to model the fine-grained trajectory. Compared to ACT, RISE exhibits a broader action distribution and can succeed twice in task 1.

Moreover, maintaining consistent source object pose relative to gripper is challenging, both during data collection and inference. This inherent variability in contact-rich manipulation tasks frequently leads to pose shifts, posing significant challenges to the algorithm’s generalization. In summary, both ACT and RISE fail to accurately model the search trajectory.

C. Gated RGBD-Augmented Pose Diffusion Policy

As shown in Table I and Table II, while PoseDP achieves high accuracy in tasks 1 to 5, its performance significantly degrades in task 6 due to the small size of the USB (Type-C) connector and micro insertion clearance. This result demonstrates that the excessive pose estimation noise prevents PoseDP from learning complex insertion trajectory. In contrast, the proposed gated RGBD-augmented pose diffusion policy (RPDP) attains a 100% success rate under standard conditions and maintains a 80% success rate even in out-of-distribution scenarios.

As shown in Fig. 6, the train and test trajectories of task 6 are visualized. The source object undergoes insertion along the target object’s z-axis. It is evident that the train

trajectories exhibit significant noise, making it challenging for the PoseDP to accurately model the insertion trajectory. However, the proposed RPDP incorporates RGBD images to aid pose features, enabling the algorithm to model complex insertion trajectories from noisy train data. In addition, we also demonstrated the position of the source object in the target object coordinate after insertion in the train/test set. The comparative analysis of train/test trajectories and post-insertion relative position (Fig. 6) reveals a pronounced divergence in the noise distributions of estimated poses between the train/test datasets. This demonstrates RPDP’s high robustness to variations in pose estimation noise. In out-of-distribution cases, we observed that when the USB port becomes occluded, the model exhibits confusion, leading to degraded success rates. Under standard conditions, for the tasks 1 to 5, RPDP achieves a success rate similar to that of the PoseDP. This occurs because these tasks are less affected by noise (Fig. 2(a)), making the auxiliary visual features less impactful. Furthermore, performance degrades in out-of-distribution cases due to limited generalization capability of visual features.

D. Ablation Study

In this section, we perform ablation studies for the DPE, GIE and PRGF.

As shown in Table III and Table IV, PoseDP w/ MLP utilizes MLP to extract pose features; PoseDP w/ DPE utilizes disentangled pose encoder to extract pose features; RPDP w/ Cat directly concatenate pose features and image features; RPDP w/ PRGF uses pose-guided residual gated fusion module to handle the pose features and image features.

Disentangled Pose Encoder In Table III and Table IV, the disentangled pose encoder achieves a higher success rate than MLP encoder. The reason is that the DPE encodes rotation and translation separately for more accurate action prediction. Our experimental observations indicate that the use of the MLP encoder may induces jamming during the insertion process, consequently preventing full insertion.

Goal-Conditioned RGBD Image Encoder In this study, the RGBD information is introduced to aid the prediction of the complex search trajectory. As shown in Table III, compared with PoseDP, while the direct concatenation of pose features and image features leads to performance degradation in tasks 1 – 5, it achieves significant improvement in task 6. This demonstrates that incorporating visual features enables the policy to model complex search trajectory despite noisy input conditions. For tasks 1 – 5, the performance

TABLE III
THE ABLATION STUDY OF OUR METHODS.

Methods	1	2	3	4	5	6	Average
PoseDP w/ MLP	100	70	90	90	60	20	71.7
PoseDP w/ DPE	100	100	90	100	70	30	81.7
RPDP w/ Cat	100	80	60	80	30	60	68.3
RPDP w/ PRGF	100	100	90	90	70	100	91.7

TABLE IV
THE ABLATION STUDY OF OUR METHODS. (OUT OF DISTRIBUTION)

Methods	1	2	3	4	5	6	Average
PoseDP w/ MLP	90	70	80	70	40	20	61.7
PoseDP w/ DPE	90	100	90	90	60	30	76.7
RPDP w/ Cat	70	70	40	70	20	50	53.3
RPDP w/ PRGF	80	90	70	90	60	80	78.3

decline occurs because the high-dimensional image features dominates the low-dimensional pose representations.

With Pose-Guided Residual Gated Fusion (PRGF) module, RPDP w/ PRGF shows slight performance degradation in tasks 1 – 5 than pose-only methods. This suggests that for these tasks, where pose observations alone provide sufficient information for successful completion, the introduction of visual features may cause potential overfitting. Conversely, RPDP w/ PRGF in task 6 demonstrates significantly improved robustness. The USB (Type-C) insertion task is sensitive to pose estimation noise, making pose-only methods unable to learn meaningful insertion trajectories from noisy observations. In contrast, visual features provide complementary geometric constraints that enhance robustness.

Pose-Guided Residual Gated Fusion As shown in Table III and Table IV, compared with direct concatenating pose features and image features, RPDP w/ PRGF achieves a higher average success rate. The mean value of gating weights is computed, and shown in Fig. 7. The analysis of the gating weights reveals significantly higher visual feature utilization in task 6 compared to task 4, with progressive increase during contact/search phases. This demonstrates: (1) PRGF is capable of dynamically selecting visual features based on pose observation; (2) Visual features can enhance the ability of the policy to model complex insertion trajectories from noisy data.

E. Further Analysis

Here, we try to address the following research questions:

(1) Why can our methods accomplish precise insertion tasks with hand-eye calibration error and robotic repeatability error? Cobot Mobile ALOHA utilizes the low-cost robotic arm, whose repeatability is 1 mm [36]. And the hand-eye calibration error is about 2 mm, which is included in T_b^c (Alg. 1). The repeatability error is included in T_b^e (Alg. 1). However, interestingly, our methods are still capable of completing the insertion task with a clearance of 0.01 mm. We argue that the proposed methods can model the complex trajectory during the insertion process, which is crucial for precise manipulation. In addition, the PoseDP can be considered as a pose-based servo controller, whereas RPDP integrates visual feedback with pose-based servo controller, forming a hybrid framework. Furthermore, both PoseDP and

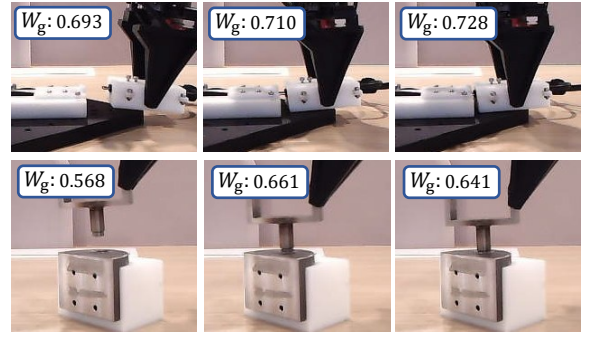


Fig. 7. The gating weights W_g during the insertion process (Top: task 6; Bottom: task 4).

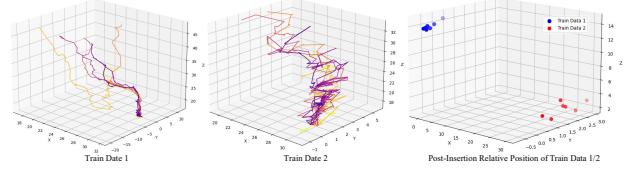


Fig. 8. Visualization of the trajectory and the post-insertion relative position of train data 1/2 (task 2; Unit: Millimeter).

RPDP only focus on the source and target objects, and both achieve closed-loop control.

(2) How does the pose estimation noise affect the algorithm’s performance? Train data collected in real-world inevitably contains noise. As illustrated in Fig. 8, we visualize the trajectories from train data 1/2, which exhibit significant divergence in post-insertion relative position. It is obvious that train data 2 contains more noise. Our experiments reveal that the PoseDP trained on data 1 achieve 100% success rate, while that trained on data 2 only reach 60% success rate. This demonstrates the importance of data quality for algorithm’s performance.

(3) Runtime Analysis On an NVIDIA RTX 4060 GPU, PoseDP requires approximately 70 ms per prediction, while RPDP takes about 140 ms per prediction.

F. Discussion and Limitation

In this paper, we propose the pose-only diffusion policy and gated RGBD-augmented pose diffusion policy. Different from the previous RL methods, we use a passive compliance controller instead of introducing force information to the policy learning. Our approach is more focused on object-centric precise manipulation trajectories, which can achieve better generalization. Force feedback may exhibit configuration sensitivity. Pose variations in either the source or target object induce force distribution shifts, compromising policy generalization. Experiments show that our methods can handle contact-rich and precise manipulation tasks, with generalization and efficiency. Nevertheless, the proposed methods have some limitations.

This study focuses on objects for which pose estimation is feasible, while neglecting small-sized objects (e.g., screw) that cannot be reliably estimated. For such small objects, the incorporation of tactile information would be necessary. Although the force information isn’t used in the proposed methods, it is still very important in contact-rich tasks,

especially for the quick reactive behavior. How to use force information reasonably with generalization ability will be an interesting topic. Furthermore, the object pose tracking may fail due to occlusion during manipulation. Therefore, introducing an additional camera for active observation and pose tracking could effectively address this issue.

V. CONCLUSION

In this paper, we explore to design the pose-guided imitation learning method for precise insertion tasks. The disentangled pose encoder is proposed to extract pose features. The goal-conditioned RGBD image encoder and the pose-guided residual gated fusion are proposed to aid the pose features for complex trajectory modeling. The proposed methods are evaluated in 6 tasks, and significantly outperforms currently imitation learning methods with impressive generalization. In addition, our methods only requires 7 – 10 demonstrations for each task. We hope this work inspires the precise and contact-rich manipulation in real-world policy learning.

In future work, it would be an interesting research direction to introduce tactile/force information to the pose-guided imitation learning.

REFERENCES

- [1] K. Ota, D. K. Jha, S. Jain, B. Yezounis, R. Corcodel, Y. Shukla, A. Bronars, and D. Romeres, "Autonomous robotic assembly: From part singulation to precise assembly," *arXiv preprint arXiv:2406.05331*, 2024.
- [2] S. Dong, D. K. Jha, D. Romeres, S. Kim, D. Nikovski, and A. Rodriguez, "Tactile-rl for insertion: Generalization to objects of unknown geometry," in *2021 IEEE International Conference on Robotics and Automation (ICRA)*, pp. 6437–6443, IEEE, 2021.
- [3] G. Schoettler, A. Nair, J. Luo, S. Bahl, J. A. Ojea, E. Solowjow, and S. Levine, "Deep reinforcement learning for industrial insertion tasks with visual inputs and natural rewards. in 2020 IEEE," in *RSJ International Conference on Intelligent Robots and Systems (IROS)*, pp. 5548–5555.
- [4] C. C. Beltran-Hernandez, D. Petit, I. G. Ramirez-Alpizar, T. Nishi, S. Kikuchi, T. Matsubara, and K. Harada, "Learning force control for contact-rich manipulation tasks with rigid position-controlled robots," *IEEE Robotics and Automation Letters*, vol. 5, no. 4, pp. 5709–5716, 2020.
- [5] X. Ma and D. Xu, "Automated robotic assembly of shaft sleeve based on reinforcement learning," *The International Journal of Advanced Manufacturing Technology*, vol. 132, no. 3, pp. 1453–1463, 2024.
- [6] V. Mnih, K. Kavukcuoglu, D. Silver, A. A. Rusu, J. Veness, M. G. Bellemare, A. Graves, M. Riedmiller, A. K. Fidjeland, G. Ostrovski, et al., "Human-level control through deep reinforcement learning," *nature*, vol. 518, no. 7540, pp. 529–533, 2015.
- [7] T. Z. Zhao, J. Tompson, D. Driess, P. Florence, K. Ghasemipour, C. Finn, and A. Wahid, "Aloha unleashed: A simple recipe for robot dexterity," *arXiv preprint arXiv:2410.13126*, 2024.
- [8] C. Chi, Z. Xu, S. Feng, E. Cousineau, Y. Du, B. Burchfiel, R. Tedrake, and S. Song, "Diffusion policy: Visuomotor policy learning via action diffusion," *The International Journal of Robotics Research*, p. 02783649241273668, 2023.
- [9] C. Wang, H. Fang, H.-S. Fang, and C. Lu, "Rise: 3d perception makes real-world robot imitation simple and effective," *arXiv preprint arXiv:2404.12281*, 2024.
- [10] A. Goyal, J. Xu, Y. Guo, V. Blukis, Y.-W. Chao, and D. Fox, "Rvt: Robotic view transformer for 3d object manipulation," in *Conference on Robot Learning*, pp. 694–710, PMLR, 2023.
- [11] A. Mandlekar, S. Nasiriany, B. Wen, I. Akinola, Y. Narang, L. Fan, Y. Zhu, and D. Fox, "Mimicgen: A data generation system for scalable robot learning using human demonstrations," *arXiv preprint arXiv:2310.17596*, 2023.
- [12] M. J. Kim, K. Pertsch, S. Karamcheti, T. Xiao, A. Balakrishna, S. Nair, R. Rafailov, E. Foster, G. Lam, P. Sanketi, et al., "Openvla: An open-source vision-language-action model," *arXiv preprint arXiv:2406.09246*, 2024.
- [13] Y. Zhu, A. Joshi, P. Stone, and Y. Zhu, "Viola: Imitation learning for vision-based manipulation with object proposal priors," in *Conference on Robot Learning*, pp. 1199–1210, PMLR, 2023.
- [14] B. Wen, W. Lian, K. Bekris, and S. Schaal, "You only demonstrate once: Category-level manipulation from single visual demonstration," *arXiv preprint arXiv:2201.12716*, 2022.
- [15] C.-C. Hsu, B. Wen, J. Xu, Y. Narang, X. Wang, Y. Zhu, J. Biswas, and S. Birchfield, "Spot: Se (3) pose trajectory diffusion for object-centric manipulation," *arXiv preprint arXiv:2411.00965*, 2024.
- [16] M. Xu, Z. Xu, Y. Xu, C. Chi, G. Wetzstein, M. Veloso, and S. Song, "Flow as the cross-domain manipulation interface," *arXiv preprint arXiv:2407.15208*, 2024.
- [17] C. Yuan, C. Wen, T. Zhang, and Y. Gao, "General flow as foundation affordance for scalable robot learning," *arXiv preprint arXiv:2401.11439*, 2024.
- [18] Y. Zhu, A. Lim, P. Stone, and Y. Zhu, "Vision-based manipulation from single human video with open-world object graphs," *arXiv preprint arXiv:2405.20321*, 2024.
- [19] G. Papagiannis and E. Johns, "Miles: Making imitation learning easy with self-supervision," *arXiv preprint arXiv:2410.19693*, 2024.
- [20] M. T. Mason, "Toward robotic manipulation," *Annual Review of Control, Robotics, and Autonomous Systems*, vol. 1, no. 1, pp. 1–28, 2018.
- [21] G. Thomas, M. Chien, A. Tamar, J. A. Ojea, and P. Abbeel, "Learning robotic assembly from cad," in *2018 IEEE International Conference on Robotics and Automation (ICRA)*, pp. 3524–3531, IEEE, 2018.
- [22] G. Schoettler, A. Nair, J. A. Ojea, S. Levine, and E. Solowjow, "Meta-reinforcement learning for robotic industrial insertion tasks," in *2020 IEEE/RSJ International Conference on Intelligent Robots and Systems (IROS)*, pp. 9728–9735, IEEE, 2020.
- [23] X. Zhang, S. Jin, C. Wang, X. Zhu, and M. Tomizuka, "Learning insertion primitives with discrete-continuous hybrid action space for robotic assembly tasks," in *2022 International conference on robotics and automation (ICRA)*, pp. 9881–9887, IEEE, 2022.
- [24] T. Z. Zhao, V. Kumar, S. Levine, and C. Finn, "Learning fine-grained bimanual manipulation with low-cost hardware," *arXiv preprint arXiv:2304.13705*, 2023.
- [25] M. Shridhar, L. Manuelli, and D. Fox, "Perceiver-actor: A multi-task transformer for robotic manipulation," in *Conference on Robot Learning*, pp. 785–799, PMLR, 2023.
- [26] Y. Ze, G. Zhang, K. Zhang, C. Hu, M. Wang, and H. Xu, "3d diffusion policy: Generalizable visuomotor policy learning via simple 3d representations," in *ICRA 2024 Workshop on 3D Visual Representations for Robot Manipulation*, 2024.
- [27] W. Huang, C. Wang, Y. Li, R. Zhang, and L. Fei-Fei, "Rekep: Spatio-temporal reasoning of relational keypoint constraints for robotic manipulation," *arXiv preprint arXiv:2409.01652*, 2024.
- [28] B. Wen, W. Yang, J. Kautz, and S. Birchfield, "Foundationpose: Unified 6d pose estimation and tracking of novel objects," in *Proceedings of the IEEE/CVF Conference on Computer Vision and Pattern Recognition*, pp. 17868–17879, 2024.
- [29] Z. Li, G. Wang, and X. Ji, "Cdpn: Coordinates-based disentangled pose network for real-time rgb-based 6-dof object pose estimation," in *Proceedings of the IEEE/CVF international conference on computer vision*, pp. 7678–7687, 2019.
- [30] G. Wang, F. Manhardt, F. Tombari, and X. Ji, "Gdr-net: Geometry-guided direct regression network for monocular 6d object pose estimation," in *Proceedings of the IEEE/CVF Conference on Computer Vision and Pattern Recognition*, pp. 16611–16621, 2021.
- [31] J. Ho, A. Jain, and P. Abbeel, "Denoising diffusion probabilistic models," *Advances in neural information processing systems*, vol. 33, pp. 6840–6851, 2020.
- [32] J. Song, C. Meng, and S. Ermon, "Denoising diffusion implicit models," *arXiv preprint arXiv:2010.02502*, 2020.
- [33] H. Kim, Y. Ohmura, and Y. Kuniyoshi, "Goal-conditioned dual-action imitation learning for dexterous dual-arm robot manipulation," *IEEE Transactions on Robotics*, 2024.
- [34] K. He, X. Zhang, S. Ren, and J. Sun, "Deep residual learning for image recognition," in *Proceedings of the IEEE conference on computer vision and pattern recognition*, pp. 770–778, 2016.

- [35] A. Dosovitskiy, L. Beyer, A. Kolesnikov, D. Weissenborn, X. Zhai, T. Unterthiner, M. Dehghani, M. Minderer, G. Heigold, S. Gelly, *et al.*, “An image is worth 16x16 words: Transformers for image recognition at scale,” *arXiv preprint arXiv:2010.11929*, 2020.
- [36] S. Liu, L. Wu, B. Li, H. Tan, H. Chen, Z. Wang, K. Xu, H. Su, and J. Zhu, “Rdt-1b: a diffusion foundation model for bimanual manipulation,” *arXiv preprint arXiv:2410.07864*, 2024.